

Interactive interpretation of 3D surfaces in field-based geosciences using mobile devices - concepts, challenges and applications

Melanie Kröhnert^{a,*}, Christian Kehl^e, Sophie Viseur^b, Simon J. Buckley^{c,d}

^a*Institute for Photogrammetry & Remote Sensing, TU Dresden, Helmholtzstr. 10, 01069 Dresden, Germany*

^b*Aix Marseille Université, CNRS, IRD, CEREGE UM 34, Dept. Sedimentary and Reservoir Systems, 13001 Marseille, France*

^c*Uni Research AS – CIPR, Nygårdsgaten 112, 5008 Bergen, Norway*

^d*Department of Earth Science, University of Bergen, Allégaten 41, 5007 Bergen, Norway*

^e*Danmarks Tekniske Universitet, DTU Compute, Richard Petersens Plads, Building 321/208, 2800 Kongens Lyngby, Denmark*

Abstract

Keywords: discrete geometry, surface reconstruction, volume reconstruction, surface parameterization, digital outcrops

2010 MSC: 00-01, 99-00

1. Introduction

A considerable number of domains within the geosciences rely on digitised natural observations and their interpretation to steer and constrain numerical models. Published (semi-)automatic interpretation methods [1, 2] emerged within the past decade that support the digital documentation of observations and interpretations. These advanced interpretation techniques require increasingly complex computing that is restricted to office-based work environments, which poses a problem for field-based studies. Domains such as hydrology, geology or glaciology (as illustrated in fig. 1) hence established multi-stage procedures where observations are taken manually in the field and later digitised in

*Corresponding author

Email addresses: melanie.kroehnert@tu-dresden.de (Melanie Kröhnert), chke@dtu.dk (Christian Kehl), viseur@cerege.fr (Sophie Viseur), Simon.Buckley@uni.no (Simon J. Buckley)

the office. This is disadvantageous and within the referred domains and there is an increasing desire to facilitate digital interpretations in the field at the study location. Mobile computing equipment (e.g. smartphones and tablets) are one technological option to facilitate such digital field-based workflows, as shown
15 in fig. 2. These devices are nowadays ubiquitous and can easily be equipped in field-based research. Also, as seen in technical magazines and the general media, the range of available devices continuously increases, which allows to find a "fit-for-purpose" device to each specific situation. New application cases, which are demonstrated and discussed in this article, and commitment within
20 geoscience- and computer technology industry lead to an increasing interest in this cross-disciplinary domain between mobile computing and geoscientific interpretation.

[BIG IMAGE OF EXAMPLE INTERPRETATION AND ANNOTATION - possibly even two pictures, one from Chris, one from Melanie
25 Mel: do you like sketches like this one sketched by myself? maybe those pictures can act as eye catchers in our introduction?]

Next to easily available, pocket-format computing devices, the required three-dimensional base data for modern applications also need to be available and being processed in a "mobile-ready" manner. The availability of topographic 3D surface data is steadily increasing due to easy-to-use software and instrumentation for surface generation (e.g. drones, structure from motion (SfM)
30 [3] and multi-view geometry [4], satellite digital elevation models (DEMs)). Furthermore, crowdsourced data and Volunteered Geographic Information (VGI) contribute to the geoscience data inventory, being acquired by citizen scientists.

35 Domain-specific mobile software is required in order allow for data interaction on the available mobile devices. Specific challenges such as power consumption, multi-manufacturer support, smart sensor utilisation and device intercommunication distinguish mobile software from common desktop software. This leads to a very different electronics design of tablets and smartphones compared
40 to desktop PCs and laptops. In return, this means that existing approaches for digital data processing and interpretation are not transferable as-is to this new

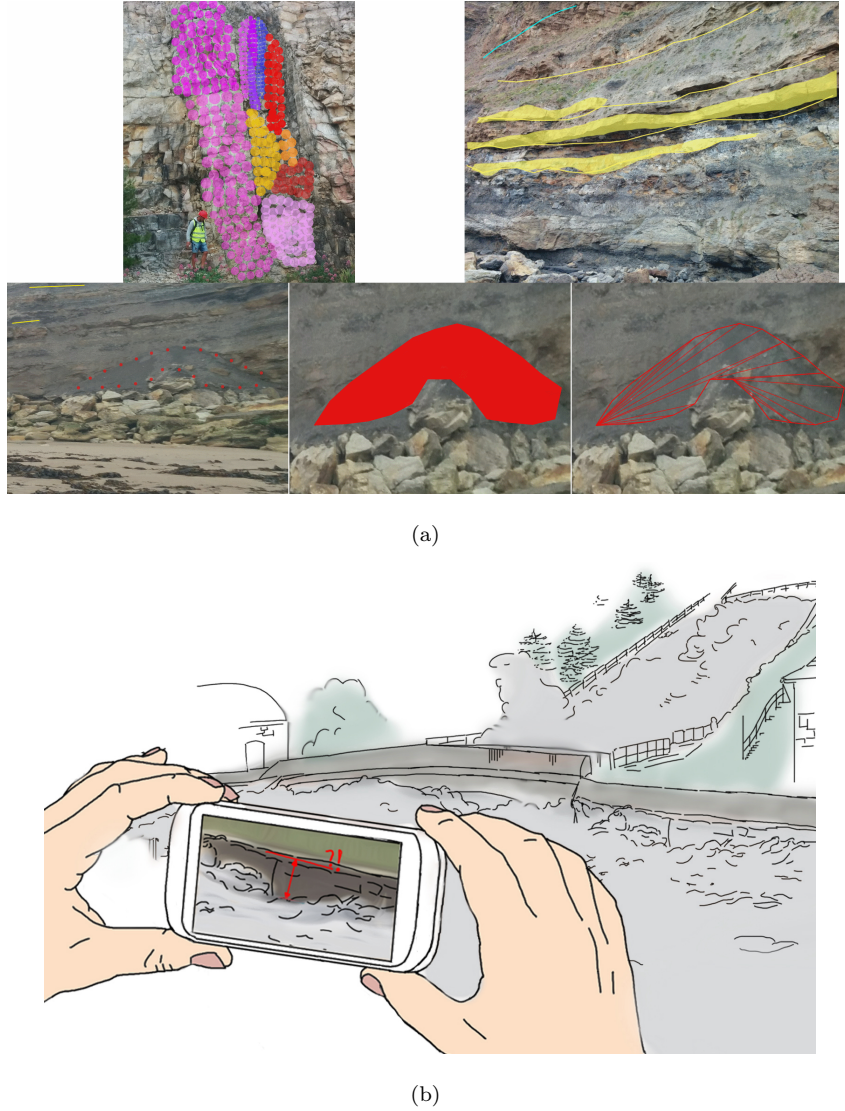


Figure 1: Illustrative examples for geological interpretation (a) and hydrological annotation (b).

computing domain. Even when considering the fast technological development, there are some challenges within mobile device software development that are rooted in the technology itself: user interfaces need to be designed specifically for touch screen interfaces, natural language interfaces and gesture interaction



Figure 2: Target application of field-based interpretation and annotation on mobile devices.

(e.g. "swipe" and "optical lens" motions). Global navigation satellite system (GNSS)-based localisation accuracy, as delivered by the integrated-circuit sensor of mobile devices, is inferior to common user expectations and requirements in geoscientific studies. The modalities of sensor data delivery (be it hardware 50 sensor or software emulation), photo capturing and processing, and the computational capabilities of mobile devices differ significantly between each vendor. Short-comings, such as inappropriate data structuring, visual object correlation and registration, increasing data volumes and the unavailability of off-the-shelf program codes, further complicate the technological development. Addressing 55 the demonstrated challenges distinguishes the mobile application development and common desktop software development for geoscience purposes. [...] You agree? Mel: got it! yes, totally agree and very good point!

This article demonstrates how the above-listed challenges can be addressed to provide, in the end, the desired added value for field-based research. This 60 demonstration addresses the 3D data annotation and interpretation for two use cases within the domains of surface hydrology and (petroleum) geology. The

content covered in the article is a detail-driven extension of earlier published research [5], focussing on extensive measurements to verify the reasoning and statements of previous studies.

65 The sections within this article adhere to the following structure: First, the
use cases are presented as opening statements to introduce field-related tasks
that are to be addressed with mobile device technology. Secondly, different 3D
surface data representations are introduced that employed within this technical
research. Thirdly, algorithmic baseline concepts that are key for interpreting 3D
70 data on mobile devices are introduced, summarising project-internal develop-
ment by the authors as well as referencing key literature on the subject. Fourth,
the algorithms are mapped to the specific mobile technologies and components.
The technologies and major parameters that impact the target use case applic-
ations are highlighted. Finally, we showcase and discuss how available mobile
75 systems are used in application scenarios from hydrology and petroleum geo-
logy to improve data analysis and integrate outdoor measurements in digital
workflows. Then, the article is finalized with some concluding remarks and a
discussion for future developments in this research trajectory.

2. Target case studies

80 TO-BE-FILLED

3. Representation basis – Geometry and Radiometry

Various representation forms for 3D terrain data are available. While early
digital systems used gridded DEMs for their simplicity and compact storage [6,
7], digital surface models (DSMs) and triangulated irregular networks (TINs) are
85 dominating most terrain-based systems for application-specific analysis [8, 9].
A useful example can be seen in [10] for glaciology, where the authors use a
triangulated digital surface model to represent a Patagonian glacier front. For
triangular surfaces, it is important to distinguish geometrically valid TINs from
polygon soup surfaces (fig. 3). While the latter is often employed in early stages

90 of mesh-based software systems due to its simplicity and ease of implementation, valid TINs are employed in mature stages of the analysis. This is because some automated analysis (e.g. auto-interpretation, volume derivation) require clean surfaces with coherently outward-oriented surface normals.

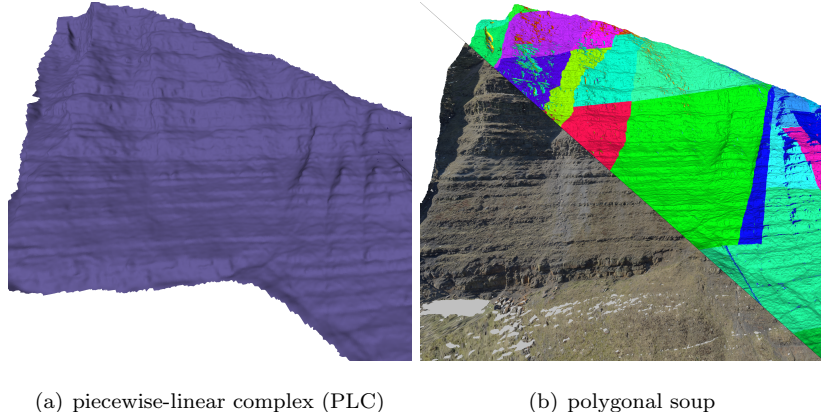


Figure 3: Illustrative distinction between valid TINs (consisting of one exclusive, smooth, closed surface) and polygonal soups. Non-textured model parts are coloured with respect to their actual segment number. Images taken from [11]

95 In geoscience domains such as petroleum geology, texture- and color information are vital for interpretation- and analysis tasks. In these cases, as demonstrated by Buckley et. al [8] and Caumon et. al [9], the TIN is supplemented with photographic information that is projected on the surface as textures. The models are referred to as digital outcrop models (DOMs) (see fig. ?? as reference depiction).

100 In contrast, other geoscience domains, such as hydrology and free surface flow management, georeferenced laser scanner point clouds and coloured point data streams provided by terrestrial photogrammetry for small- or unmanned aerial vehicle (UAV) for large-scale use cases are used. The point set surface data support tasks like coastal monitoring [12, 13], soil erosion and rain-induced 105 landslide observation, even monitoring river's topography [14] and even flood protection management [15]. Nevertheless, new approaches for low-cost and on-



Figure 4: Example of a DOM as textured triangular surface.

the-fly river monitoring [16] arise due to globally increasing flash flood events after heavy rainfalls [17] that are further addressed in section 6.1.

Since SfM became state of the art in geosciences, the acquisition of (true-)coloured "point cloud" models is not that difficult and commonly employed because of its rapid processing (compared to conventional approaches like terrestrial laser scanning (TLS)). Regarding 3D annotation, nearest neighbour analysis provides an opportunity whereby surface triangulation can be avoided.

The stated base concepts of geometric representation and radiometric texture information are also valid for mobile device software. Because of the limited processing speed of mobile chipsets, the usage of point cloud appears most common within the graphics literature (e.g. Garcia et. al [18]). The sparse vertex distribution in point clouds causes problems in the data analysis, which is why DEMs have seen a revival in the mobile computing domain. DEMs provide dense, closed geometric models that can be rendered and processed efficiently. Furthermore, with the inferior memory capacity of mobile devices in comparison to laptops and workstations, the possible compression options for point clouds and DEMs are advantageous. Base mapping applications such as Google Maps use DEMs, derived from light detection and range (lidar) or satellite data [19], as their main topographic data representation. Other 3D processing systems on mobile devices within the geosciences, such as "Outcrop" and Geological Registration and Interpretation Toolset (GRIT), employ genuine textured triangulated DSM.

The chosen form of model representation significantly impacts the algorithms
¹³⁰ and analytical capabilities employed on the mobile device. Although all algorithms presented in this article work on either form of representation, some of the algorithms favour the treatment of triangulated surfaces (e.g. image-to-geometry registration, guided interpretation), while others clearly favour point-based representations (e.g. rendering).

¹³⁵ 4. Algorithms

This section demonstrates novel- as well as existing algorithms and methods on mobile devices that provide the basis for case-specific field-based annotation, interpretation and analysis shown in section 2. As mentioned before, the effectiveness of each algorithm depends on the applied model representation.

¹⁴⁰ 4.1. Image-to-geometry registration

Image-to-geometry algorithms aim at registering 2D images to a given 3D surface, providing a transformation from the 2D image coordinate system to 3D model coordinate system as follows:

$$P' = \begin{pmatrix} u \\ v \\ w \end{pmatrix} = [R_{3,3}|T_{1,3}] \cdot P \quad (1)$$

$$P = \begin{pmatrix} x \\ y \\ z \end{pmatrix} \quad (2)$$

$$P' \in \mathbb{R}^2 = \frac{P'}{w} \quad (3)$$

$R_{3,3}$.. rotation matrix, $T_{1,3}$.. translation vector, P .. 3D point in object space,
¹⁴⁵ P' .. 2D projected point in image space, (u, v, w) .. 2D image coordinates,
 (x, y, z) .. 3D world coordinates

Using this coordinate system transformation in combination with a known interior camera orientation, it is possible to project each image on the surface. Specific objects outlined in the image, such as image-based interpretations, can
150 also be mapped on the surface. In the geosciences, these algorithms are employed to create a direct correlation between 3D model and the screen- or image space on which annotations and interpretations are based on [20].

Amongst the published literature, feature-based registration algorithms are most common. Here, salient points (e.g. SIFT, SURF, Harris corners) or edges
155 within the photograph and rendered image of the target 3D model are used to establish an image-to-image correlation.

In order to establish a 2D–3D correlation, there are two prevalent approaches available: for triangle mesh models, the 2D feature locations within the rendered image are raycasted using the virtual camera’s vanishing point, the imaging
160 plane, and the 3D surface model (see fig. 2 in [20]). The intersection between the ray and a triangle within the mesh results in the correlated 3D coordinate of the 2D feature. An alternative approach is needed for point-based models because the raycasting does not apply to point representations (i.e. points cannot be intersected directly due to their zero-extent). The alternative approach often
165 applied (see [21, 22?]) employs smart rendering techniques that virtually expand the point into an area feature (e.g. blob, disk or sphere), which is subsequently rendered into a depth map. Afterwards, the 3D coordinate of a 2D feature can be inferred directly from the depth map. Though cleverly utilising graphics technology, this approach is limited by an accuracy-to-speed
170 trade-off: low-resolution and low-quantisation depth maps introduce artificial accuracy errors in the registration process, whereas high-resolution depth maps (above 512^2 pixels) cost considerable performance in the image generation. This last point is particularly important when employing depth map algorithms on mobile devices.

175 When 2D–3D point pairs are established, the coordinates are normalized and put into a least-squares optimization system, where the target is to determine the exterior camera parameters ($t_x, t_y, t_z, \psi, \varphi, \theta$) from the 2D–3D point-based

equation system. Non-linear optimisation systems (e.g. Levenberg-Marquardt) are applied to estimate the desired parameter set [23]. The whole process can easily be executed on mobile devices [20]. One of the prevalent practical challenges when employing feature-based image-to-geometry registration is to achieve a reliable feature correlation, which is often achieved by introducing application-specific constraints (e.g. horizon alignment, straight-edge enforcement or object outlines).

Feature-based registration is the most common approach for establishing image-to-geometry correlation on mobile devices due to its implementation simplicity, its rapid execution speed, its option for application-specific constraints and the wealth of available code that can be used. Examples for the application of the technique are ample within the literature, ranging from augmented reality [24, 25] over field geology [20, 26] to surface hydrology [16, 27]. These mobile apps utilize the open-source library *OpenCV4Android*¹, which is also employed in this work². Problems in real-world cases are posed to this technique from imaging variances, resulting in reduced reliability (i.e. failing to determine any camera parameters) and stability (i.e. determining different parameters for the same sets of images) [28]. A completely alternative technique to feature-based methods is Mutual Information (MI) [29, 30]. MI performs a pixel-wise comparison between the photo I_{2D} and the 2D rendering of the 3D scene I'_{3D} and aims at minimizing the image discrepancies (i.e. $\text{argmin} \Delta(I_{2D}, I'_{3D})$). The technique uses information theory quantities such as self-information and entropy in order to compare the similarity of both image (see [31] for further applications of MI within the geosciences). In contrast to feature-based techniques, MI faces challenges in the optimization process: the optimization of a 7 degree-of-freedom equation system ($t_x, t_y, t_z, \psi, \varphi, \theta, f$, for f being the focal length) is unstable and prone to rest in local function minima. Only few optimisation solvers are known that can solve such equation systems reliably and provide stable results -

¹OpenCV4Android 2.4.10 - <https://opencv.org/platforms/android/>

²OpenCV4Android extensions at https://github.com/CKehl/opencv4Android_extension

most notably NEWUOA (i.e. Powell’s method[32]) used in [30]. As these stable solvers are not available in modern- and mobile-device programming languages, the use of MI is currently prohibited for mobile platforms.

While the task of image-to-geometry registration can be offloaded to remote computers in the network, it is advantageous to perform the registration on the mobile device itself. This is because, in the overall target of model interpretation, the interaction and actual interpretation (as explained in section 4.4) is more intuitive for the user when being performed on photos and images. If the registration of the images is done on the mobile device, it allows for direct feedback and ad-hoc visual quality checks of the interpretations on the underlying 3D surface model (see fig. 7 in [26]). Furthermore, as shown by measurements in section 5.3, it can be argued that 2D interpretation more energy efficient than direct 3D interpretations. Lastly, in settings where network access and offline processing is prohibited, an on-device registration procedure is without alternatives.

4.2. Mesh-based rendering

Rendering a surface model in this context refers to the image generation of the 3D data by projective rasterization to the 2D image plane of a virtual camera. This process is performed on mobile devices for the purpose of model presentation as well as for the generation of a synthetic reference image for image-to-geometry registration. Furthermore, it can be used to synthesize an image from available 3D data for interpretation and annotation in 2D.

Algorithms for rendering textured triangulated surfaces are well-known amongst technology-affine personnel. In the common rendering pipeline, the textured mesh is transferred as a set of (attributed) vertices and primitive sets (e.g. triangles, polygons) to the graphics processing unit (GPU). The virtual camera is set up using the pre-defined view projection matrix while the graphics primitives are repositioned using the model-related transformation matrix. The rasterizer projects the available 3D information into the camera plane and performs hidden-surface removal. The result is a discrete-space pixel represent-

ation. Modern programmable shaders allow in-time vertex decompression (see [33]) as well as texture decompression (see section 5.2). Available textures are mapped as images on the surface using the texture coordinate vertex attributes.
²⁴⁰ The mesh-based rendering algorithms employed on desktop computers are analogous to mobile devices, whereas the technological details are posing the actual challenges.

4.3. A novel approach to mobile point-based rendering

In comparison to mesh-based rendering, simple point projection seems to be a nice alternative saving computational resources and efforts for post-processing
²⁴⁵ concerning outlier removal due to falsely surface reconstruction (e.g. blobs due to critic point normals) [Chris: what do you refer to as "critic point normals"](#) ?. Thus, we simply project object points onto an image plane using perspective projection, assuming a distortion-free ideal camera with centred principle point. Thus, the camera matrix \mathbf{K} equals identity matrix \mathbf{I} and can be neglected in
²⁵⁰ the following equations (based on Szeliski(2010) [please insert proper reference here to avoid confusion](#)).

First, applying a six-parameter transformation transfers three-dimensional object points from world reference frame \vec{X}_W into a 3D camera system \vec{X}_c using

$$\vec{X}_c = \mathbf{R} (\vec{X}_W - \vec{X}_0) \quad (4)$$

where \mathbf{R} is a 3×3 orthonormal rotation matrix and \vec{X}_0 the translation vector to camera's projection center. For simplicity, the usage of the planar Cartesian UTM system with x pointing to the east and y pointing to the north with
²⁵⁵ respect to the prevalent zone number. For z component, the height over the Earth Gravitational Model 1996 (EGM96) is advisable to use.

Counting for homogeneous coordinates, we can describe the relation between

camera \vec{X}_c and image coordinates \tilde{x} involving their depth components.

$$\begin{pmatrix} \tilde{u} \\ \tilde{v} \\ c_c \end{pmatrix} = \begin{pmatrix} x_c \\ y_c \\ z_c \end{pmatrix} \quad (5)$$

For camera's imaging plane, we introduce the constant c_c that defines the distance between camera's sensor and projection center in [mm], which equals focal length f . To separate camera sensor system and image system, we use the term c_c when talking about sensor [mm], and f for digital image coordinates [px]. For conversion, c_c must be divided by the sensor's pixel pitch. Chris: The normalization of the projected points to homogeneous coordinates is key in the further processing. This is analogous to the image-to-geometry project in eq. 1, where the projection variable w is replaced with the camera constant c_c .

Chris: For 3D to 2D projection, homogeneous coordinates must be divided by their depth components resulting in inhomogeneous coordinates. [remove following equations, as we have them already.]

$$\vec{X}_{Cam} = \begin{pmatrix} \frac{\tilde{u}}{c_c} \\ \frac{\tilde{v}}{c_c} \\ 1 \end{pmatrix} = \begin{pmatrix} \frac{x_c}{z_c} \\ \frac{y_c}{z_c} \\ 1 \end{pmatrix} \quad (6)$$

Thus, two-dimensional coordinates can be described with

$$\begin{pmatrix} \tilde{u} \\ \tilde{v} \end{pmatrix} = \begin{pmatrix} \frac{x_c}{z_c} \cdot c_c \\ \frac{y_c}{z_c} \cdot c_c \end{pmatrix} \quad (7)$$

For a final transformation of 2D sensor coordinates into image pixels, we need to shift the image coordinate system to the origin to left upper corner and scale the coordinates from global units in meters per pixel using p_s . Thus, we derive image coordinates (u, v) for an ideal camera using

$$\begin{pmatrix} u \\ v \end{pmatrix} = \frac{1}{p_s} \begin{pmatrix} \frac{x_c}{z_c} \cdot c_c - u_0 \\ \frac{y_c}{z_c} \cdot c_c - v_0 \end{pmatrix} \quad (8)$$

Chris: end of current check-read - looks good so far.

4.3.1. Calculation of 3D bounding box of interest and image plane

Referring to the described use case of situation-based water level determination using a smartphone-camera based gauge (6.1), we need to define a region of interest regarding 3D point projection to render only user's field of view (figure 5). Thus, bounding box defining points to be projected must be calculated using camera position and orientation from fused smartphone sensors. Thereby it must be noted, that the heading is used for viewing direction only, tilt and roll are excluded. Because of uncertainties regarding exterior information (section 5.1), bounding box must be expanded to cover more object space than described by sensors as well as cameras field of view. Because of possible noise due to positioning, constants r and dh describe the domain of projection center's uncertainties parallel to image plane. For errors in depth, we define the correction $c = \frac{r}{\tan(H)}$ for shifting the projection center along camera axis.

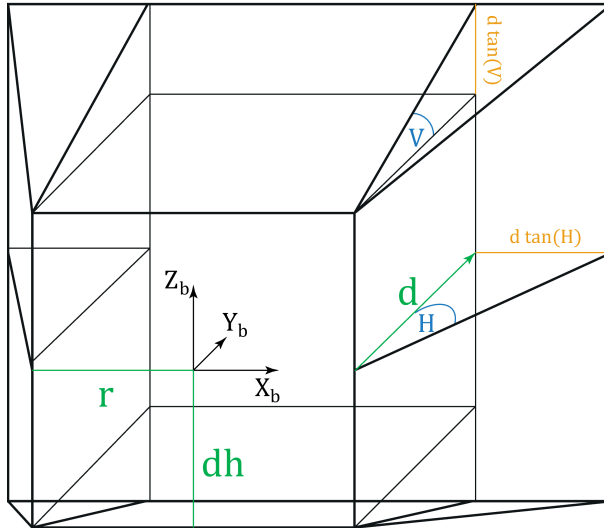


Figure 5: Bounding box definition.

The box is widened by the horizontal H and vertical V opening angles with a fixed depth d . In order to generate reference data for image-2-geometry intersection to annotate 3D data by mobile imagery, the lateral accuracy given by

mobile positioning system as well as the prevalent camera characteristics solve
²⁹⁰ for the mentioned parameters. For camera based gauging, we set $d = 200[m]$. Regarding 3D point projection, each potential point will be checked laying in the box. Therefore, additional tiling of the 3D data set is advisable. Using the defined frustum of a pyramid as region of interest with local reference system, the image plane for 3D point rendering can be defined by perspective projection
²⁹⁵ of the remote xz plane (5) with

$$\vec{X}_b = \begin{pmatrix} -r - d \tan H \\ d \\ dh + d \tan V \end{pmatrix}$$

for bounding box' background plane upper left and

$$\vec{X}_b = \begin{pmatrix} r + d \tan H \\ d \\ -dh - d \tan V \end{pmatrix}$$

lower right corner. Its height equals the height component in world reference frame z_w . Because of pyramid frustum, we finally must eliminate outer points between the smaller front and larger rear plane considering the eight extremes.

³⁰⁰ workflow for outer point removal necessary?

4.3.2. Pyramid approach for depth filtering

Because of a limited range of pixels with defined size inside a image plane it seems to be obvious that in most cases more than one 3D object points corresponds to the same image pixel. Due to inhomogeneous coordinates it is
³⁰⁵ not possible to figure out afterwards which points are in foreground compared to the camera distances and which ones are behind and so not visible. This problem can easily be solved during point cloud projection described above by a simple camera-to-object distance check. However, one problem still remains in case of e.g. glass fronts with lacking information (in TLS due to deflected

lidar or SfM when having homogeneous surfaces) or small archs (see figure 7)
 Then, points might be visible pointing away from camera projection center. On
 the one hand, point normals may solve the problem but due to data acquisition
 technique and model's complexity, they are more or less easy to derive (**Sattler
 zitieren**). Remedyng image pyramids are a nice alternative approach used in
 this case. Therefore, multiple synthetic images are generated with step-by-step
 adjustment of p_s (see eq. 8), commonly by doubling which resulting in halve
 numbers of image rows and columns per layer. Than, the algorithm verifies if
 two pixels corresponds in two subsequent layers, preserving edges (figure 6,7).

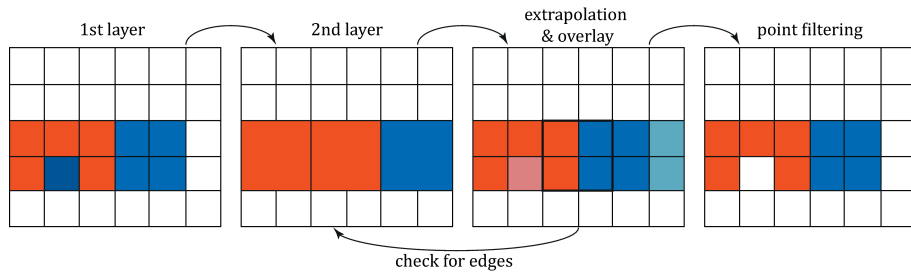


Figure 6: Visualisation of hierarchical depth filtering to handle point occlusions.

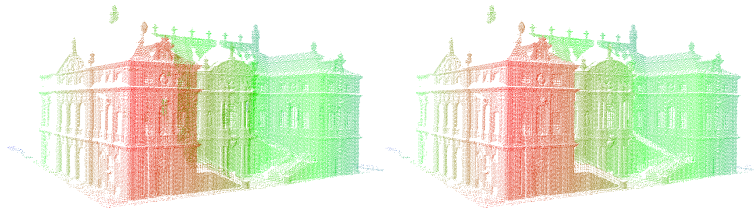


Figure 7: Left, actually obscured visible 3D points close to archs and windows. Right, edge preserving result after filtering.

4.3.3. Filling gaps due to missing points

Because of pixel size and image plane definition with a specific resolution
 (that depends in case of 6.1.2 on smartphone camera's resolution) there will be
 still gaps inbetween projected points (see figure 7, right). To fill these gaps,

we recommend to use a simple nearest neighbour approach using binary search [34] in 3D domain to fill these gaps applying weights to average 3D points color attributes depending on their euclidean distances. For this, thresholds for maximum distances between 3D points must be applied to avoid unreasonable gap-filling. Exemplary for use case 6.1 results before and after gap filling are visualised in figure 8.



Figure 8: Fill image gaps using nearest neighbour binary search in 3D domain.

4.4. Interpretation and annotation

Interpretation and annotation techniques aim to map geometries (e.g. lines, polygons) of domain-specific information to the 3D base surface. The mapped geometries are used to delineate interest boundaries or to segment the surface into semantically meaningful units.

In hydrological cases, line interpretations are commonly used to mark current water levels as well as high-tide or high-surge water levels. Health monitoring of dykes and levees can use line interpretations to mark cracks within surge defense structures. In geological cases, a mixture of line- and polygon geometries are used. Line interpretations are more commonly related to structural rock features (e.g. cracks, fractures, fault zone boundaries, stratigraphic boundaries), while polygonal area segmentation are more common in sedimentology (e.g. depositional elements, sedimentary objects, sediment facies). That being said,

application of the geometries within geology is flexible, as observed in the case of fault facies that use area marks for structural features.

The delineation and mapping can be performed in various ways, depending
345 on the geometric representation of the 3D base surface geometry. Point clouds and 3D TINs can be annotated in directly in 3D. In such application, area markings can be directly embedded as vertex attributes while closest-vertex searches (for point clouds) or view-surface intersections (for TINs) provide the corners for line interpretations. The largest problems with such direct-3D approach on mobile devices are the data size of the underlying surface and complexity of neighbourhood searches. Nearest neighbour search has a computational complexity of $O(nd)$, where $d = 3$ for 3D surfaces and n being the number of vertices in the dataset. This results in non-interactive execution times for 3D vertex marking on mobile devices with real-world datasets (with $n \geq 10^7$). Performing interpretations in 3D on mobile devices also require supportive interaction schemes, including intuitive and easy-access switches between 3D space orientation and actual point selection for the user. Other issues for general direct-3D surface interpretation include the a sparse vertex distribution and open, non-convex geometry (being a particular problem for TINs), surface occlusion and intricate problems related to curved surfaces, where the euclidean vertex distance and geodesic distance along the surface can differ significantly.
355
360

Utilising the aforementioned image-to-geometry registration (section 4.1), the given issues of direct-3D interpretation and 3D interaction can be circumvented. The raster image interpretation is computationally more efficient due to
365 the gridded data arrangement and easier to use for novice practitioners on mobile devices. The interpretation geometries are generated as 2D vector graphics elements, which are projected on the 3D surface after the image registration using the estimated external camera orientation or pose.

5. Technology

370 *5.1. Sensors*

5.1.1. Localization

- references: ...

5.1.2. Orientation

- stability IMU (see 3D-NO)

375 • precision IMU

5.1.3. Parameter sensitivity

5.2. Graphics

As shown in section 4, 3D rendering constitutes key algorithms for surface-based interpretation and annotation. Mobile devices can implement the rendering in two distinct ways: directly on the device using the integrated GPU, or via remote rendering over the network and the transmission of images.

In cases where the app’s target environment are urban settings and locations of well-developed infrastructure, the mobile device can utilise the wireless network connectivity and apply *remote rendering* for the image generation. This allows externalising the rendering tasks for 3D models and supplementary data (as in Ponchio et al. [33]), where the mobile device only submits render requests (supplemented with current view parameters) and receives the generated image. This makes the usage of larger and higher-resolution models more tangible as they are not affected by mobile device limitations. In contrast, the limitations on remote rendering are set by the requested target image size- and resolution, the target refresh rate, and the limited bandwidth of the mobile network [?]. Moreover, the process is agnostic to the specific mobile device specification sending the request, making the rendering process work across all major mobile device system manufacturers (e.g. Google, Apple, Microsoft/Nokia). A positive side affect as a result of remote rendering is the reduced energy consumptions

(see section 5.3 for details), which allows for applying advanced algorithms for sensor tracking in localisation and orientation.

The internet access may be restricted or expensive to establish (e.g. up to 70 euro per month³) for other outdoor applications in remote areas). Thus, 400 outdoor applications operating in remote areas are prohibited from web-based rendering and need to perform rendering on the device. In this case, the 3D data reside in the device memory and the rendering process is affected by the performance-restricted mobile device hardware.

The emergence of mobile graphics libraries such as Khronos graphics library 405 for embedded systems (GLES), Vulcan and Open Scene Graph on Android⁴, as well as the continuously improving mobile graphics chipsets (e.g. Qualcomm Adreno, ARM Mali, NVIDIA Tegra), makes on-device rendering a feasible option for apps targeting field-based geosciences. Pinhead example software for field-based studies using mobile device graphics on some way are OpenWater- 410 Level [16], GRIT [35] and Outcrop [36]. Mobile graphics itself is still a hot topic with is the principle science discipline of computer graphics, visualisation and virtual reality [18, 33, 37]. Scaling up the principle graphics lab results (in terms of data size, image resolution and texture utilisation) to actual requirements within the geosciences is a prime challenge. Although mobile manufacturers provide more powerful devices to allow for more data and higher 415 resolutions, mobile devices need to sacrifice capabilities such as sensor availability as well as physical size and weight in order to provide larger memory space and higher-performance processors. Examples for this trade-off manufacturing can be seen in special-purpose and high-performance tablets such as NVIDIA 420 Shield⁵, Project Tango resp. ARCore⁶ and Google Pixel C⁷. Another problem

³see www.skydsl.eu, skyDSL2+ flatrate with 30 MBit/s download

⁴osgAndroid - original at <https://github.com/miragetech/osgAndroid>, extended by the second author at <https://github.com/CKehl/osgAndroid>

⁵NVIDIA Shield - <https://developer.nvidia.com/develop4shield>

⁶Google Augmented Reality - <https://developers.google.com/ar/>

⁷Google Pixel C- <https://www.android.com/tablets/pixel-c/>

rarely considered in scientific literature on mobile graphics is power consumption, which is of pivot importance for field practitioners (see section 5.3). A specific problem that impacts geoscientists and domain experts with respect to on-device rendering settings is the trade-off between app responsiveness, image quality, hardware utilization and cross-device operability illustrated in fig. 9.

425

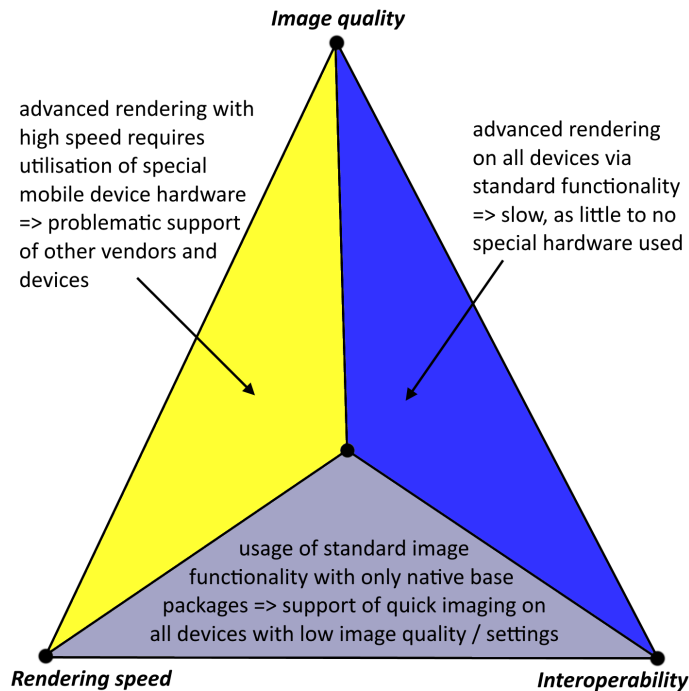


Figure 9: Conflicting trinity of image (i.e. rendering) quality, rendering speed (a collective term in this context for special hardware utilisation and responsiveness) and interoperability (between devices of the same vendor as well as between vendors).

430

In interviews conducted amongst field geologists at the Dept. of Earth Science at the University of Bergen, a major demand from the target user base of such mobile app (i.e. domain experts and practitioners) is a facilitated interoperability between Android, Microsoft and Apple devices. This demand potentially originates from the platform-agnostic functioning of common geoscience software (e.g. geographic information systems (GIS), geomodelling software) on desktop computers for Apple and Windows. On the other hand, app respons-

iveness and high image quality are amongst the next common priorities behind interoperability. Moreover, the interview geoscientists expect to receive for improved quality when advanced equipment (e.g. special-purpose tablets, novel-
435 and high-performance tablets) is available. Both demands are conflicting because making use of specialised hardware (e.g. GPU Computing such as CUDA⁸ for image processing [38, 39], texture compression [40]) in turn means reducing the range of devices being able to operate the software. Still, these specialised
440 technologies are key to achieve the required responsiveness and image quality.

5.3. Power consumption

Power consumption is an important metric for mobile field application, which is at the same time also distinct to the mobile device platform. This metric governs the operation time of an app in an outdoor field setting for specific
445 studies. In application domains such as field geology, the target operation time is in the range of four hours to eight hours without device recharging. The original operation time can be extended with external battery packs, although there is a limit of how many battery packs can be taken into the field before their total weight renders the mobile device impractical as a field tool.

450 We measured the energy consumption of *Open Water Level* and *GRIT* in realistic settings for case studies in waterline detection and field interpretation. Measuring the power consumption on an app-specific level is not supported by default on mobile devices. Formerly, the power consumption has only been assessed on a hardware component level [41]. This study utilised the Trepn Profiler⁹, which is currently the only known app on Android devices that facilitate app-specific measurements. Trepn Profiler also allows for the simultaneous logging of technical indicators (e.g. GPU- and central processing unit (CPU) load, memory consumption, CPU temperature), which is used in this study to draw higher-level conclusions on the utilisation of the apps. The presented meas-
455

⁸CUDA - <https://developer.nvidia.com/cuda-zone>

⁹Trepn Profiler - <https://developer.qualcomm.com/software/trepn-power-profiler>

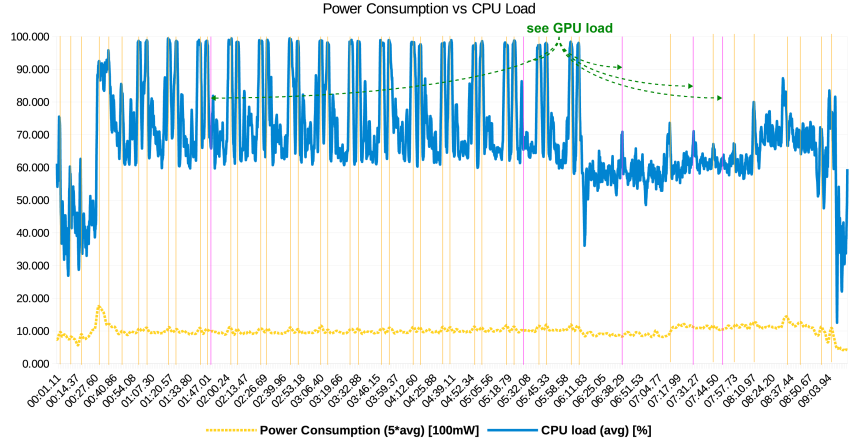
460 urements were obtained on a Google Nexus 5 smartphone (4-core ARM CPU, Qualcomm Adreno GPU). Additional measurements have been obtained with Samsung S8 (8-core ARM CPU, 20-core Mali GPU) which can be located in the supplementary data of this article.

465 In an initial test, we compare the power consumption relative to the CPU- and GPU load. Our hypothesis was that a higher GPU load results in an increased power consumption compared to CPU-dominated operations, because mobile GPUs draw more power than CPUs to realise the increased graphics performance. The results are shown for GRIT and for OpenWaterLevel, split in CPU (fig. 10) and GPU (fig. 11) contributions.

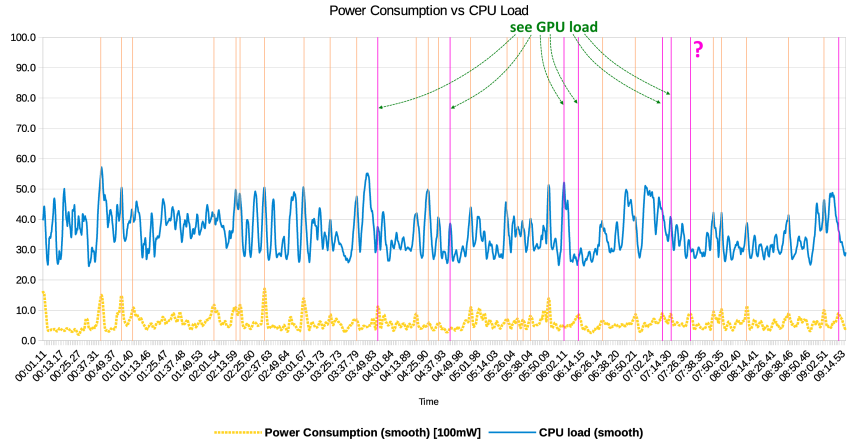
470 In both apps, a clear dependency with CPU load and power consumption is observable. We can therefore conclude that the mobile processors adapt their clock frequency when less operations are performed, which leads to a reduced power consumption. When comparing CPU-related and GPU related states, it is concluded that while the CPU drives the average power consumption, the 475 GPU (being used for rendering images and annotations in images) drives the peak power consumption.

480 GRIT has two distinct clusters of operations, each dominated by either 2D- or 3D tasks, which makes a difference in the ratio of CPU load to GPU load. The 2D operation mode includes tasks such as photo acquisition and the image-based photo interpretation, whereas the 3D operations include the image-to-geometry registration [26] and the 3D outcrop viewer. Previous figures 10(b) and 11(b) depict the 2D-dominated cases, whereas fig. 12 shows the power consumption relationships in 3D-dominated cases.

485 As clearly observable in fig. 14(a) in comparison to fig. 14(b), the 3D operations result in a drastic energy cost, raising the average power consumption by around 1220.21 mW. In contrast to novice expectation, the CPU load also increases in a 3D data processing setting because the main processors deliver the geometric- and texture data to the GPU. Additionally, for the Google Nexus 5 smartphone, the CPU needs to decompress the texture image files, resulting 490 in a higher processing load.

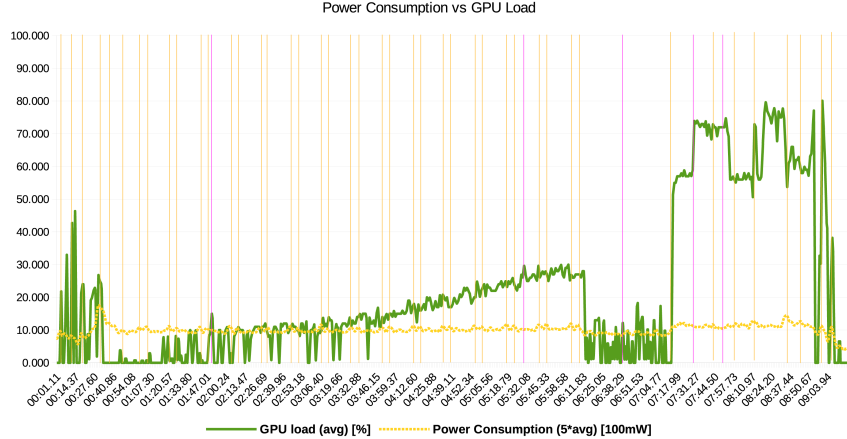


(a) Open Water Levels

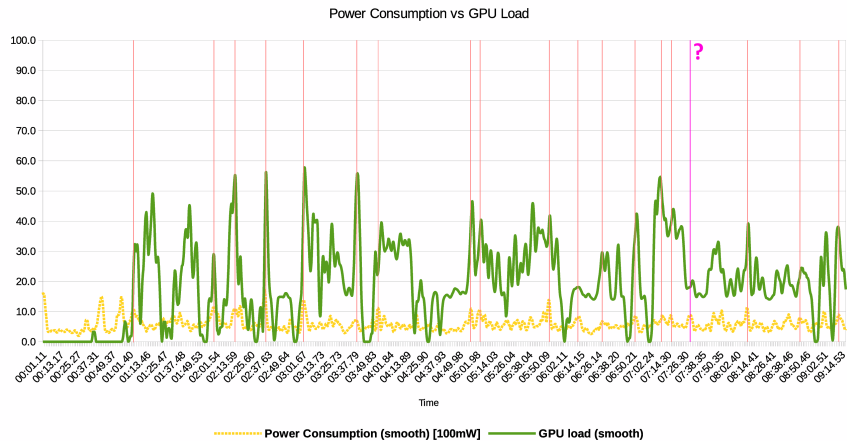


(b) GRIT

Figure 10: Diagram of power measurements with respect to the CPU load, comparing Open Water Levels and GRIT in 2D mode. The less saturated lines show direct correlations between peak CPU load and peak power consumption, while fully saturated lines show missing peak correlations where they are expected.

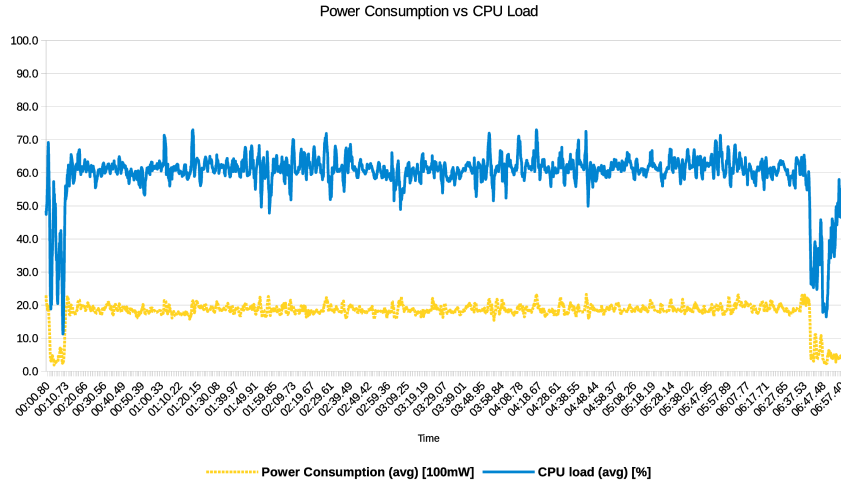


(a) Open Water Levels

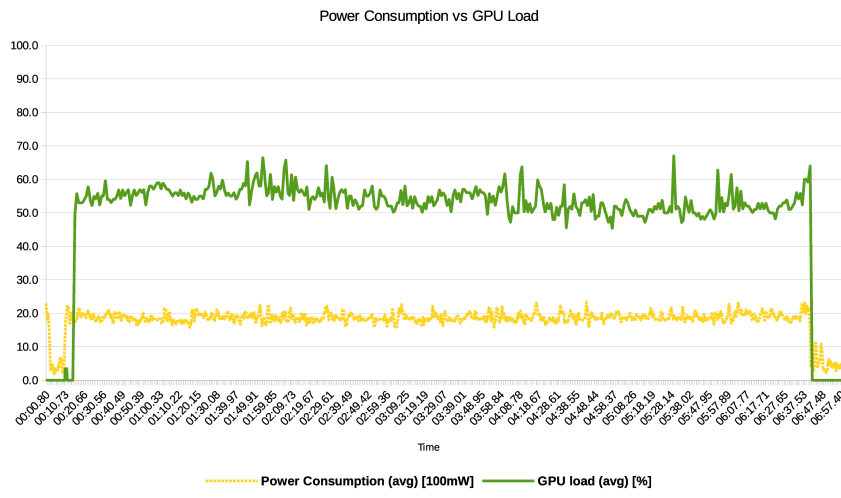


(b) GRIT

Figure 11: Diagram of power measurements with respect to the GPU load, comparing Open Water Levels and GRIT in 2D mode. The less saturated lines show good peak correlations between GPU load and power consumption; fully saturated lines show missing peak correlations. Compared to fig. 10, the majority of missing peak correlations from the CPU band are explained by increased GPU utilisation.



(a) Power to CPU



(b) Power to GPU

Figure 12: Diagram of power measurements with respect to the CPU- & GPU load of GRIT in 3D mode.

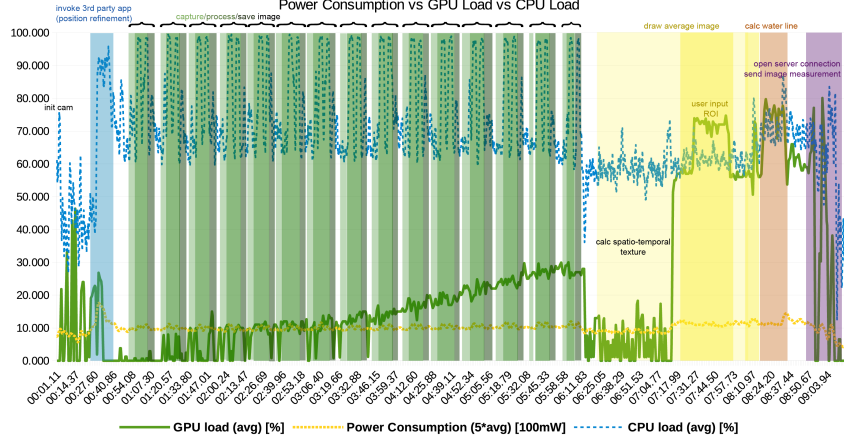
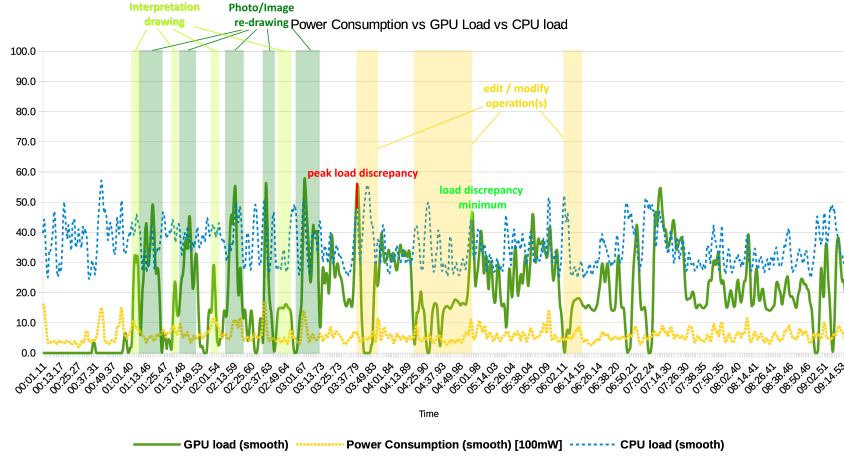


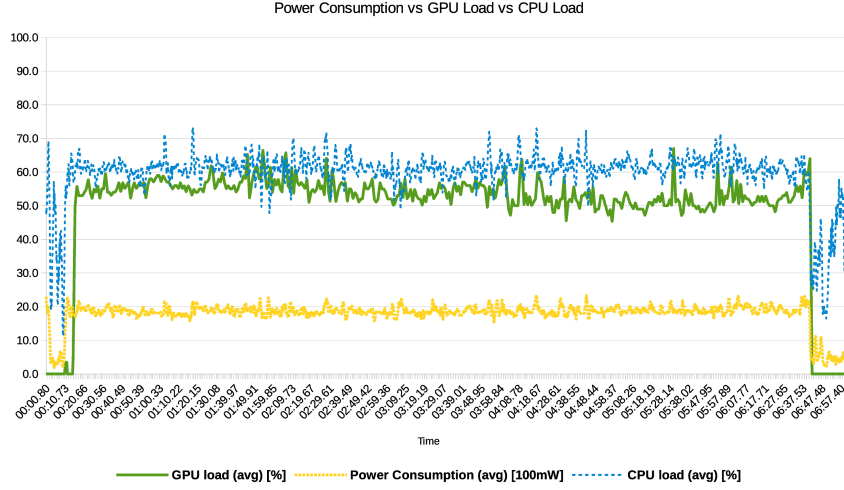
Figure 13: Integrated diagram of power consumption, CPU- & GPU load of Open Water Levels in 2D mode.

Figure 5.3 visualises the relationship of power consumption, CPU, as well as GPU for 2D data processing in Open Water Levels. For water line detection, a spatio-temporal texture must be calculated using time lapse images. Thus, the CPU load locally exceeds and falls significantly for each single frame processing (here 15 peaks for 15 images). Unlike CPU behaviour, GPU load is steadily increasing while storing each co-registered image. After image processing, both CPU as well as GPU load are released whereas app modifications via user interface leads, as expected, once more to higher loads.

The conclusions of this power consumption study for field apps is manifold. We obtained benchmark measurements for specific target apps in hydrology (Open Water Levels) and geology (GRIT), and explained how to replicate the study on Android devices with other field apps in the future. For Open Water Levels, the app can be operated on an average of 1090.41 milliampere per hour (natively measured in milliampere), allowing a theoretical operability of 2.11 hours on the Google Nexus 5. For GRIT, we have to distinguish between the mode in which it is operated: when conducting 2D operations, the app consumes 568.50 milliwatt per hour, which results in an operation time of 14.56



(a) 2D mode



(b) 3D mode

Figure 14: Integrated diagram of power consumption, CPU- & GPU load of GRIT in 2D- & 3D mode.

hours at an average current of 3.6V. When making full usage of the 3D capabilities of GRIT all the time, the average power consumption rises to 1788.80 milliwatt per hour, which results in an operation time of only 4.63 hours at an average current of 3.6V. The applied current for the GRIT measurements is of theoretical nature, applied because the measurements were taken in watt exclusively while the battery capacity of mobile devices is commonly given in milliampercere hours. Furthermore, we highlight these measurements as being the *theoretical* operation time because most users have other apps and background services open on their mobile device that simultaneously consume power, further reducing the operation time. Lastly, as stated by Carroll et al. [41], the app-specific consumption (in particular with "visual apps" and the sensor applications) also depends on the screen brightness and the sensor usage. Key measures on power consumption, and related metrics of processor temperature and memory usage, are given in table 1 for GRIT and table 2 for Open Water Levels.

In more general terms applicable to the geoscience domain, the study shows that users need to be aware of what data they are dealing with in order to get the maximum operation time and most efficient workload done during the operations. This will have distinct implications for fieldwork planning for expert users and practitioners, as they can modify their study plan to first collect photos, observations and interpretations from several viewpoints of their study object and then use 3D operation features "in burst" for visual checks and data interrogation before moving on to further study locations. Insufficient planning and an overuse of 3D field app features can reduce the effective "digital fieldwork" time using GRIT to 9.26 hours at best when carrying one external battery pack. Also, with this measure we want to highlight that the operation time error in the measurements is significant because we need to assume an average current of 3.6V, which may be far off when comparing the measurements to *Open Water Level*. Considering the CPU load behaviour in 3D-mode of GRIT, we can also hypothesize about the positive impact of utilising hardware-specific operations, such as GPU texture decompression, on the energy consumption: while

using the GPU requires generally more power, it is also more efficient in operations such as texture decompression, therefore potentially having a positive affect on the overall power consumption of 3D mobile field apps.

Table 1: Average measurements of GRIT

metric	2D ops.	3D ops.
power consumption [mW/h]	568.59	1788.80
power consumption [mA/h 3.6V]	157.94	496.89
memory usage (avg.) [GB]	1.746	1.721
temperature [°C]	49.91	52.05

Table 2: Average measurements of Open Water Levels

metric	Google Nexus 5	Samsung S8
power consumption [mA/h]	1090.41	?
memory usage (avg.) [GB]	1.543	?
temperature [°C]	58.55	?

6. Applications and Requirements

Due to the increasing usability of mobile devices for in the field annotations, several use cases concerning geosciences has become apparent. In the following, two essential

6.1. Derivation of hydrological parameters: Water level gauging

The last decade is characterized by a continued increase of globally devastating flash floods after heavy rainfalls. Even smallest creeks turned into hazardous streams causing flooding and landslides. Conventional gauging stations provide precise information about water levels measured over a short time period. State

of the art techniques for administrative observation comprise water pressure sensors, floating gauges and conventional tide gauges. They are characterised by long-term stability and outdoor robustness providing accuracies of several millimeters up to one centimeter [42]. Averaged over defined time intervals, it is advisable to remain cautious regarding these accuracies may be too optimistic [43].

Because of high costs in purchase and maintenance, gauging stations with complex sensing devices must be sparsely installed. A prime example here is the hydrological network in Saxony, Germany. Here, 184 gauging stations are installed for permanent observation on 154 of 259 rivers rising from small, medium and large catchments [44, 45]. Thus, around a third is not monitored neither during flood events when the most protection is required. Recently, commercial smartphone applications arose to enable crowd-sourcing based water level estimation for, among other things, such cases [46, 47]. But all of them have one thing in common: the water level is entered manually by engaged citizen scientists finding and photographing tide gauges close to rivers that makes - on the one hand a potential danger to themselves (f.e. by sudden landslides), and still limits on the other the approaches to open and visible gauges.

Improvements in this sense can be achieved through *image-2-geometry intersection* and 3D annotation for automatic water level determination without reference gauges for almost every situation regarding running waters. For this, the smartphone application *Open Water Level* that bases on the freely available open source camera framework *Open Camera* [48]. Open Water Level allows for free stationing water line detection using short hand held time-lapse image sequences [16]. To interpret these, image measurements must be transformed into object space. Thus, exterior information needs to be provided by smartphone sensors for orientation and positioning.

6.1.1. Requirements applying to the sensors

To solve the task of autonomous water level determination on running rivers f.e. emergency cases using *image-2-geometry intersection*, citizen scientists po-

sition and orientation must be know. As figured out in 5, smartphone sensors accuracies for orientation and location are highly dependent on user's environment. Especially the strong correlation of heading and disturbing magnetic sources may be a issue must be solved specifically related to running rivers where metal railings usually exists. Similar effects can also be noted using high-end IMU systems for instance autonomous car navigation. But the magnetic influences inside cars are almost stable and can be calibrated during the drive (advanced navigation manual). For smartphone orientation, the magnetic strengths attaching the phone may change substantially in short time. A typical scenario would be: a citizen scientist walks along street, taking his phone inside the baggage close to metallic keys. While walking he passes several street lamps, signs, etc. Finally, he arrives at a bridge over a urban river, takes out the phone, looks down to the river and records the time lapse image sequence a few centimetres above a metallic railing. Meanwhile, several cars passing the same bridge. In this simple use case, the magnetic field around the smartphone changes countless times due to several unpredictable disturbances ([table mag disturb](#)) [49].

The heading angle has the highest influence compared to pitch and roll regarding 2D image and 3D object data registration. For this, a so-called synthetic image is rendered from colored 3D reference point clouds using scientist's location and orientation to define a situation-dependent bounding box of points to be projected onto image plane with respect to depth and indentations (see [27]). Thereby the heading defines the rotation of the depth direction, as a false angle gives a false viewing direction resulting in a synthetic image that has no similarity or only a little with the time lapse sequence. However, in case of no similarity and thus no possible solution for *image-2-geometry intersection*, simply no water level can be calculated. But in case of slight overlapping, there might be image matches but with very bad distribution that impedes a correct positioning ([fig heading test](#)) and may lead to even worse results of false water levels.

It is obvious that a second source for destructive results exists: the absolute geo-positioning using smartphones currently installed GNSS receivers. In urban

scenes with several shadow effects due to high-rise buildings, errors of several
615 meters in latitude and up to more than 30 meters in height are highly possible where even the weather has impact [50, 49, 51]. It is likely that, in the near future, smartphone's GNSS modules will be improved solving lateral accuracies of 50 centimetres [52].

For now, possible relief might come including other sources for positioning like
620 digital elevation models for simple height correction or invoke map services that allows the user for position refinement. For this, some APIs are already provided by Google ([quellen](#)) but they are rather cost-expensive by extensive accessing. Another upcoming option is including barometers in sensor fusion, altitude can be measured within three meters [53] but for now, they are not a standard.

- 625
- (table, observation heading during water line detection outside → check magnetic strengthens and there changes over short times)
 - (figure/table, sensitivity analysis → heading changed in terms of 10 degrees, what does it make for)

6.1.2. Requirements applying to the scenario

- 630
- *online processing and position refinement: need online connection*
 - *image quality for water line detection: influence of image resolution, lighting, ...)*
 - available approach to address the task

6.2. Field Geology

635 The goal of geological fieldtrips is to gather insight in the rock record and the structural- and sedimentary rock architecture of a given location. Rock architecture can be studied within subsurface seismic records, but this approach suffers from inferior imaging resolutions and physical limitations of the surveying technique. Therefore, surface outcrops are used for the study. Outcrops can be
640 scanned with modern equipment (e.g. lidar [8, 54], drones [55] and SfM [56]) to

generate digital surface representations. The most common representations of digital outcrops are coloured point clouds and textured TINs.

The geological aspect is introduced by interpreting the outcrop models. In this case, interpretations refer to (i) line marks for separating stratigraphic layers, (ii) surface-projected polygons to highlight structural- and sedimentary facies or specific architectural elements and (iii) minor ticks (e.g. lines, points, patterns) to indicate depositional attributes such as deposition orientation or grain geometry. The interpretations was until recently performed in a two-step process: sketches are drawn by hand in the field to document the field geologist's observation of the architecture. After the fieldtrip, the observations are digitalised in the office by transferring the sketched architecture on the available digital outcrop. From there on, further study goals (e.g. geomodelling) are pursued. As recently published, this workflow is currently being transformed into an integrated digital workflow in the field using mobile devices (see [57] for further details).

Geological interpretations can be documented on various scales, but from observations of the author most interpretations are conducted on medium-range. This results in an average observation distance for architectural interpretations of between $100m$ to $500m$ to document individual depositional elements and further distances of around $400m$ to $1400m$ to document the overall stratigraphic framework of an outcrop. Therefore, as a result of perspective observations, the required lateral localisation accuracy is in the range of $\leq 2.5m$ for the individual element setting and $\leq 8m$ for the wide-angle stratigraphic setting. While achieving the former resolution can still be challenging with mobile sensors (see section 5.1.1), the latter resolution is almost guaranteed for GPS localisation.

The more important problem is in the vertical resolution: the vertical observation position has, especially in close-distance observations, a drastic impact on the view perspective. Even more important, a vertical localisation error of $\geq 1.5m$ may result in positioning the mobile device "under ground", making any image-based registration impossible. It is this vertical accuracy that is crucial for mobile device interpretation systems to work. Several improvements,

such as DEMs and barometric altitude [26], have been proposed to reduce the vertical positioning error while there is still room for novel research proposals to provide more accurate vertical positioning or ground-based constraints on the
675 altitude estimation.

One of the dominant challenges for digital field geology is the free availability of 3D surface models. Currently, research groups in the domain (e.g. from the University of Manchester, Durham University, University of Aberdeen, University of Bergen and UniResearch CIPR) are building their own digital outcrop
680 databases. Due to the strong industry involvement, these and other databases (see SAFARI [58] and FAKTS [59]) are excluded from public access. Recent developments aim at providing digital outcrops in an open-access manner [60] to resolve the issue. Furthermore, due to the vertical positioning problem above, easy access to high- and medium resolution DEMs is important. As demonstrated by recent measurement, the usage of DEMs has a significant influence
685 on the projection accuracy of image-based interpretation on mobile device towards 3D surface models [26].

One particular challenge in digital field geology is the treatment of environmental changes. Digital outcrops are infrequently collected and the textured
690 models are used for field study all across the year. Therefore, in image registration terms, there is a drastic difference in local illumination, moisture content as well as fog and snow between acquired 3D surface models and the outcrop images collected during field trips. The issue has been previously discussed in terms of illumination differences [28], but drastic changes in terms of fog and
695 moisture are still problematic to treat. Therefore, it is advisable to collect digital outcrop models for prominent locations in different seasonal conditions to allow for variety in model selection when planning field trips.

Currently available systems that provide digital outcrop interpretation capabilities on mobile devices in 3D include GRIT [35] and Outcrop [36], though
700 earlier prototypes have been demonstrated [61]. Outcrop, developed by Centre Européen de Recherche et d'Enseignement des Géosciences de l'Environnement (CEREGE) at Aix-Marseille Université, is a mobile device app for Android

devices that is able to load and process various forms of numerical outcrops. Its major focus is the documentation of structural features (e.g. fault areas, fractures and rock deformations) on outcrops using line interpretations. Furthermore,
705 it is possible to pin extended note annotations to the model. GRIT, developed as a collaboration between UniResearch AS CIPR, University of Bergen, University of Aberdeen and CEREGE, is a mobile device app for Android devices that can handle large-area digital outcrops of tens of kilometres in surface length in
710 3D. Its major focus is the documentation of the sedimentary- and stratigraphic architecture (e.g. strata boundaries, depositional object envelopes, facies areas) on outcrops via lines, polygons and brushes. The interpretations are mapped in a 2D-3D interplay between outcrop surface and field photograph.

[comparison photo: GRIT and Outcrop]

- 715 • ~~recap: task to be solved~~
- ~~main requirements for (location- and orientation) sensor accuracy and geometric accuracy~~
- ~~specific requirements to this use case: data availability; illumination; network inavailability~~
- 720 • ~~available approach to address the task~~

6.3. Virtual Field Trips

- 725 • recap: task to be solved
- ~~main requirements for (location- and orientation) sensor accuracy and geometric accuracy~~
- ~~specific requirements to this use case: data availability; illumination; network inavailability~~
- ~~available approach to address the task~~

7. Conclusions

This article assessed the possibility of interactive interpretation and annotation of 3D outcrops on mobile devices in multiple geoscientific domains. Due to the research effort in recent years, novel mobile applications such as Open-WaterLevels for surface hydrology and GRIT for field geology were introduced to the community to bridge the gap between lab assessment and outdoor field work for data interpretation. This article also showed further application areas that build upon mobile device technology and the interactive annotation of 3D surface data for geoscientific problem solving.

McCaffery et al. proposed the use of mobile devices for field interpretation in geology in 2005 [7]. The technological specifics of mobile device app development hampered the progress on this goal for years. Only recent advancements in efficient treatment of 3D data [5], algorithmic proposals for image-to-geometry registration (see [24, 26]) and on-device 3D rendering (as presented in [37] and in this article for point-based surface) specifically designed for mobile devices make the actual use for geoscientific applications in the field possible. The utilisation of crowdsourced VGI and introduction of mobile devices as low-cost measuring devices for real-world problems [62] contribute to the acceptance of this mobile device technological development within the geoscientific community. Computer Vision challenges such as image registration under changing illumination conditions and with reduced image resolution can be viewed as "sufficiently solved" to make photogrammetric- and vision-based algorithms applicable to real-world outdoor settings, while still leaving space for improvement and quality and performance.

The measurements found in this article as well as its related studies suggest that localisation and orientation of mobile device sensors with respect to the application-specific accuracy requirements is a persisting challenge. The sensors employed by low-cost devices have accuracy limitations. Sensor filtering- and fusion techniques are required to even moderately consider the use of such sensor data. Environmental effects such as device-internal heating processes and the

system-internal handling of sensor initialisation further complicate the calibration of such sensors without user involvement.

760 Furthermore, this study gives a representative overview about the energy consumption of mobile apps employing 3D surfaces, computer vision and computer graphics procedures. It was shown that the distinction between 2D- and 3D data used by mobile apps significantly drives the power consumption, and therefore the operation time of the mobile field apps during a study. Means of 765 reducing the power consumption in the future have, next to extended periods of app use by domain experts, beneficial secondary effects: power-reduced main functions of the mobile app allow energy-expensive simultaneous localisation and mapping (SLAM) techniques to be used for sensor data augmentation.

770 Lastly, the treatment of vegetation within scanned- and photographed data during mobile field studies remains a challenge in the context of interactive interpretation. 3D reference data are obtained less frequent than they are used in a given outdoor setting. Vegetation itself is visually dynamic content that complicates image registration to existing 3D data, which complicates interpretations in common outdoor settings. While current procedures of data processing try to segment- and remove vegetation data from scans, it leaves the 775 mobile device app with less information to work with when registering photos. Therefore, proposing means of 3D topographic data processing that homogenizes vegetation in 3D scans and photos without removing the related data will have an impact on accurate outdoor photo registration on 3D base data.

780 **8. Discussion**

- porting existing desktop algorithms on mobile devices [quick and fast]
- pre-processing of geodata for mobile use

Acknowledgements

First, we would like to thank M.Sc. Richard Boerner from TU Munich, 785 Germany for his assistance with the development of an alternative approach for

synthetic image generation using perspective 3D to 2D image projection with respect to object space definition and to solve for point occlusions (see section 4.3). Furthermore, we want graduate the European Social Fund and the Free State of Saxony for their financial support (funding no. 100235479).

790 **References**

- [1] B. Nyberg, S. J. Buckley, J. A. Howell, R. A. Nanson, Geometric attribute and shape characterization of modern depositional elements: A quantitative {GIS} method for empirical analysis, *Computers & Geosciences* 82 (2015) 191 – 204.
- 795 [2] J. Ruiu, G. Caumon, S. Viseur, Semiautomatic interpretation of 3d sedimentological structures on geologic images: An object-based approach, *Interpretation* 3 (2015) SX63–SX74.
- [3] C. Wu, Towards linear-time incremental structure from motion, in: 2013 International Conference on 3D Vision - 3DV 2013, 2013, pp. 127–134. doi:10.1109/3DV.2013.25.
- 800 [4] M. Goesele, N. Snavely, B. Curless, H. Hoppe, S. M. Seitz, Multi-view stereo for community photo collections, in: Computer Vision, 2007. ICCV 2007. IEEE 11th International Conference on, IEEE, 2007, pp. 1–8.
- [5] M. Kröhnert, C. Kehl, H. Litschke, S. J. Buckley, Image-to-geometry registration on mobile devices - concepts, challenges and applications, in: L. Paul, G. Stanke, M. Pochanke (Eds.), 3D-NordOst, volume 20, Gesellschaft zur Förderung angewandter Informatik, 2017, pp. 99–108.
- 805 [6] I. Trinks, P. Clegg, K. McCaffrey, R. Jones, R. Hobbs, B. Holdsworth, N. Holliman, J. Imber, S. Waggett, R. Wilson, Mapping and analysing virtual outcrops, *Visual Geosciences* 10 (2005) 13–19.
- [7] K. McCaffrey, R. Jones, R. Holdsworth, R. Wilson, P. Clegg, J. Imber, N. Holliman, I. Trinks, Unlocking the spatial dimension: digital technolo-

- logies and the future of geoscience fieldwork, *Journal of the Geological Society* 162 (2005) 927–938.
- 815 [8] S. J. Buckley, J. A. Howell, H. D. Enge, T. H. Kurz, Terrestrial laser scanning in geology: data acquisition, processing and accuracy considerations, *Journal of the Geological Society* 165 (2008) 625–638.
- 820 [9] G. Caumon, G. Gray, C. Antoine, M. O. Titeux, Three-dimensional implicit stratigraphic model building from remote sensing data on tetrahedral meshes: Theory and application to a regional model of la popa basin, ne mexico, *IEEE Transactions on Geoscience and Remote Sensing* 51 (2013) 1613–1621.
- 825 [10] E. Schwalbe, H.-G. Maas, The determination of high-resolution spatio-temporal glacier motion fields from time-lapse sequences, *Earth Surface Dynamics* 5 (2017) 861–879.
- [11] C. Kehl, Visual Techniques for Geological Fieldwork using Mobile Devices, Ph.d. thesis, University of Bergen, 2017.
- 830 [12] P. Letortu, M. Jaud, P. Grandjean, J. Ammann, S. Costa, O. Maquaire, R. Davidson, N. L. Dantec, C. Delacourt, Examining high-resolution survey methods for monitoring cliff erosion at an operational scale, *GIScience & Remote Sensing* (2017) 1–20.
- 835 [13] M. Medjkane, O. Maquaire, S. Costa, T. Roulland, P. Letortu, C. Fauchard, R. Antoine, R. Davidson, High-resolution monitoring of complex coastal morphology changes: cross-efficiency of SfM and TLS-based survey (vaches-noires cliffs, normandy, france), *Landslides* (2018).
- [14] Y. Watanabe, Y. Kawahara, UAV photogrammetry for monitoring changes in river topography and vegetation, *Procedia Engineering* 154 (2016) 317–325.
- 840 [15] J. G. Leskens, C. Kehl, T. Tutenel, T. Kol, G. de Haan, G. Stelling, E. Eismann, An interactive simulation and visualization tool for flood analysis

usable for practitioners, Mitigation and Adaptation Strategies for Global Change (2015) 1–18.

- [16] M. Kröhnert, R. Meichsner, Segmentation of environmental time lapse image sequences for the determination of shore lines captured by handheld smartphone cameras, ISPRS Annals of the Photogrammetry, Remote Sensing and Spatial Information Sciences IV-2/W4 (2017) 1–8.
845
- [17] E. N. Mueller, A. Pfister, Increasing occurrence of high-intensity rainstorm events relevant for the generation of soil erosion in a temperate lowland region in central europe, Journal of Hydrology 411 (2011) 266 – 278.
- [18] S. García, R. Pagés, D. Berjón, F. Morán, Textured splat-based point clouds for rendering in handheld devices, in: Proceedings of the 20th International Conference on 3D Web Technology, Web3D '15, ACM, New York, NY, USA, 2015, pp. 227–230. URL: <http://doi.acm.org/10.1145/2775292.2782779>.
850
- [19] T. G. Farr, P. A. Rosen, E. Caro, R. Crippen, R. Duren, S. Hensley, M. Kobrick, M. Paller, E. Rodriguez, L. Roth, et al., The shuttle radar topography mission, Reviews of geophysics 45 (2007).
- [20] C. Kehl, S. Buckley, R. Gawthorpe, I. Viola, J. Howell, DIRECT IMAGE-TO-GEOMETRY REGISTRATION USING MOBILE SENSOR DATA, ISPRS Annals of Photogrammetry, Remote Sensing & Spatial Information Sciences 3 (2016) 121–128.
860
- [21] D. Sibbing, T. Sattler, B. Leibe, L. Kobbelt, Sift-realistic rendering, in: 2013 International Conference on 3D Vision - 3DV 2013, 2013, pp. 56–63.
- [22] T. Sattler, B. Leibe, L. Kobbelt, Fast image-based localization using direct 2d-to-3d matching, in: 2011 International Conference on Computer Vision, IEEE, 2011. doi:10.1109/iccv.2011.6126302.
865

- [23] P. Torr, A. Zisserman, Mlesac: A new robust estimator with application to estimating image geometry, *Computer Vision and Image Understanding* 78 (2000) 138 – 156.
- 870 [24] S. Gauglitz, C. Sweeney, J. Ventura, M. Turk, T. Hollerer, Model estimation and selection towards unconstrained real-time tracking and mapping, *Visualization and Computer Graphics, IEEE Transactions on* 20 (2014) 825–838.
- [25] C. Sweeney, J. Flynn, B. Nuernberger, M. Turk, T. Hollerer, Efficient computation of absolute pose for gravity-aware augmented reality, in: *Mixed and Augmented Reality (ISMAR), 2015 IEEE International Symposium on*, 2015, pp. 19–24.
- 875 880 [26] C. Kehl, S. J. Buckley, S. Viseur, R. L. Gawthorpe, J. R. Mullins, J. A. Howell, Mapping field photos to textured surface meshes directly on mobile devices, *The Photogrammetric Record* 32 (2017) 398–423.
- [27] R. Boerner, M. Kröhnert, Brute force matching between camera shots and synthetic images from point clouds, volume XLI-B5, 2016, pp. 771–777.
doi:doi:10.5194/isprs-archives-XLI-B5-771-2016.
- 885 [28] C. Kehl, S. J. Buckley, S. Viseur, R. L. Gawthorpe, J. A. Howell, Automatic illumination-invariant image-to-geometry registration in outdoor environments, *The Photogrammetric Record* 32 (2017) 93–118.
- [29] P. Viola, W. M. Wells, Alignment by maximization of mutual information, *International journal of computer vision* 24 (1997) 137–154.
- [30] M. Corsini, M. Dellepiane, F. Ganovelli, R. Gherardi, A. Fusello, R. Scopigno, Fully Automatic Registration of Image Sets on Approximate Geometry, *International journal of computer vision* 102 (2013) 91–111.
- 890 [31] X. Bonaventura, A. A. Sima, M. Feixas, S. J. Buckley, M. Sbert, J. A. Howell, Information measures for terrain visualization, *Computers & Geosciences* 99 (2017) 9 – 18.

- 895 [32] M. J. Powell, The newuo software for unconstrained optimization without
derivatives, in: Large-scale nonlinear optimization, Springer, 2006, pp.
255–297.
- [33] F. Ponchio, M. Dellepiane, Multiresolution and fast decompression for
optimal web-based rendering, Graphical Models 88 (2016) 1 – 11.
- 900 [34] J. L. Bentley, Multidimensional binary search trees used for associative
searching, Communications of the ACM 18 (1975) 509–517.
- [35] C. Kehl, J. R. Mullins, S. J. Buckley, R. L. Gawthorpe, J. A. Howell,
I. Viola, S. Viseur, Geological Registration and Interpretation Toolbox
(GRIT): A Visual and Interactive Approach for Geological Interpretation
905 in the Field, in: Proceedings of 2nd Virtual Geoscience Conference, 2016,
pp. 59–60.
- [36] S. Viseur, R. Roudaut, R. Bertozzi, M. Castelli, J.-L. Mari, 3d interactive
geological interpretations on digital outcrops using a touch pad, in: Vertical
Geology Conference (VGC), 2014.
- 910 [37] M. Agus, E. Gobbetti, F. Marton, G. Pintore, P.-P. Vázquez, Mobile
Graphics, in: A. Bousseau, D. Gutierrez (Eds.), EuroGraphics 2017 - Tu-
torials, The Eurographics Association, 2017. doi:10.2312/egt.20171032.
- [38] S. Heymann, K. Müller, A. Smolic, B. Froehlich, T. Wiegand, Sift im-
plementation and optimization for general-purpose gpu, Winter School of
915 Computer Graphics (WSCG) (2007).
- [39] M. A. Hudelist, C. Cobârzan, K. Schoeffmann, Opencv performance
measurements on mobile devices, in: Proceedings of International Con-
ference on Multimedia Retrieval, ICMR '14, ACM, New York, NY,
USA, 2014, pp. 479:479–479:482. URL: <http://doi.acm.org/10.1145/2578726.2578798>. doi:10.1145/2578726.2578798.

- [40] D. Chait, Using ASTC Texture Compression for Game Assets, whitepaper, NVIDIA Corporation, 2015. URL: <https://developer.nvidia.com/astc-texture-compression-for-game-assets>.
- [41] A. Carroll, G. Heiser, et al., An analysis of power consumption in a smartphone., in: USENIX annual technical conference, volume 14, Boston, MA, 2010, pp. 21–21.
- [42] S. Siedschlag, Wasserstände und Durchflüsse - messen, speichern und übertragen im digitalen Zeitalter, in: Dresdenner Wasserbauliche Mitteilungen, volume 53 of *Dresdenner Wasserbauliche Mitteilungen*, Technische Universität Dresden, Institut für Wasserbau und technische Hydromechanik, 2015. URL: <https://henry.baw.de/handle/20.500.11970/103357>.
- [43] I. Horner, B. Renard, J. L. Coz, F. Branger, H. McMillan, G. Pierrefeu, Impact of stage measurement errors on streamflow uncertainty, Water Resources Research (2018).
- [44] Saxon Flood Centre, Water levels & flow rates, 2018. URL: <https://www.umwelt.sachsen.de/umwelt/infosysteme/hwims/portal/web/wasserstand-uebersicht>, accessed: 2018-03-05.
- [45] U. Büttner, E. Wolf, Konzeption des gewässerkundlichen pegelnetzes in sachsen, 38. Dresdenner Wasserbaukolloquium 2015 Messen und Überwachen im Wasserbau und am Gewässer (2015).
- [46] S. Etter, B. Strobl, Crowdwater, 2018. URL: <http://www.crowdwater.ch/de/home/>, accessed: 2018-03-06.
- [47] Kisters, Einfach smart: App für Pegelmessung auf Knopfdruck, 2014. URL: https://www.kisters.de/fileadmin/user_upload/Wasser/Produkte/WISKI/Produktblaetter/MobileWaterTracker_de_mail.pdf, accessed: 2018-03-06.
- [48] M. Harman, Open Camera - Camera app for Android, 2017. URL: <https://sourceforge.net/projects/opencamera/>, version 1.38.

- [49] J. R. Blum, D. G. Greencorn, J. R. Cooperstock, Smartphone sensor reliability for augmented reality applications, in: K. Zheng, M. Li, H. Jiang (Eds.), *Mobile and Ubiquitous Systems: Computing, Networking, and Services*, Springer Berlin Heidelberg, Berlin, Heidelberg, 2013, pp. 233 – 248.
- [50] C. Bauer, On the (in-)accuracy of gps measures of smartphones: A study of running tracking applications, in: *Proceedings of International Conference on Advances in Mobile Computing & Multimedia*, MoMM '13, ACM, New York, NY, USA, 2013, pp. 335:335–335:341. URL: <http://doi.acm.org/10.1145/2536853.2536893>. doi:10.1145/2536853.2536893.
- [51] P. A. Zandbergen, S. J. Barbeau, Positional accuracy of assisted GPS data from high-sensitivity GPS-enabled mobile phones, *Journal of Navigation* 64 (2011) 381–399.
- [52] S. K. Moore, Superaccurate gps coming to smartphones in 2018, *IEEE Spectrum* (2017). Accessed: 2018-03-06.
- [53] G. Liu, K. M. A. Hossain, M. Iwai, M. Ito, Y. Tobe, K. Sezaki, D. Matekenya, Beyond horizontal location context: measuring elevation using smartphone's barometer, in: *Proceedings of the 2014 ACM International Joint Conference on Pervasive and Ubiquitous Computing Adjunct Publication*, ACM Press, 2014. doi:10.1145/2638728.2641670.
- [54] S. J. Buckley, E. Schwarz, V. Terlaky, J. A. Howell, R. Arnott, Combining Aerial Photogrammetry and Terrestrial Lidar for Reservoir Analog Modeling, *Photogrammetric Engineering & Remote Sensing* 76 (2010) 953–963.
- [55] T. J. Dewez, J. Leroux, S. Morelli, Uav sensing of coastal cliff topography for rock fall hazard applications, in: *Journées Aléas Gravitaires JAG 2015*, 2015.
- [56] J. Chandler, S. Buckley, Structure from motion (SFM) photogrammetry vs terrestrial laser scanning, American Geosciences Institute (AGS), 2016.

- [57] C. Kehl, J. R. Mullins, S. J. Buckley, J. A. Howell, R. L. Gawthorpe, Interpretation and mapping of geological features using mobile devices in outcrop geology - a case study of the saltwick formation, north yorkshire, uk, AGU Books - Special Issue (2018 (accepted for publication)).
- 980 [58] T. Dreyer, L.-M. Fält, T. Høy, R. Knarud, J.-L. Cuevas, et al., Sedimentary architecture of field analogues for reservoir information (SAFARI): a case study of the fluvial escanilla formation, spanish pyrenees, in: The Geological Modeling of Hydrocarbon Reservoirs and Outcrop Analogs, volume 15, International Association of Sedimentologists – Special Publications, Wiley Online Library, 1993, pp. 57–80.
- 985 [59] L. Colombera, F. Felletti, N. P. Mountney, W. D. McCaffrey, A database approach for constraining stochastic simulations of the sedimentary heterogeneity of fluvial reservoirs, AAPG bulletin 96 (2012) 2143–2166.
- 990 [60] A. J. Cawood, C. E. Bond, erock: an online, open-access repository of virtual outcrops and geological samples in 3d, in: EGU Geophysical Research Abstracts, volume 20, 2018, p. 18248.
- 995 [61] L. Hama, R. A. Ruddle, D. Paton, 3d mobile visualization techniques in field geology interpretation: Evaluation of modern tablet applications, in: AAPG Hedberg Research Conference: 3D Structural Geologic Interpretation: Earth, Mind and Machine, 2013.
- [62] A. Eltner, H. Sardemann, M. Kröhnert, E. Schwalbe, Camera based low-cost system to monitor hydrological parameters in small catchments, in: EGU General Assembly Conference Abstracts, volume 19, 2017, p. 6698.

Highlights

1000

- point 1
- point 2
- point 3
- point 4
- point 5

1005